Nanoscale Electrical Investigation of Transparent Conductive Electrodes Based on Silver Nanowire Network

Sy Hieu Pham, Anthony Ferri, Antonio Da Costa, M. Mohan, van Dang Tran, Duy Cuong Nguyen, Pascal Viville, Roberto Lazzaroni, Rachel Desfeux, Philippe Leclère

ADVANCED MATERIALS INTERFACES
www.advmatinterfaces.de

Nanoscale Electrical Investigation of Transparent Conductive Electrodes Based on Silver Nanowire Network

*Sy Hieu Pham, Anthony Ferri, Antonio Da Costa, M. M. Saj Mohan, Van Dang Tran, Duy Cuong Nguyen, Pascal Viville, Roberto Lazzaroni, Rachel Desfeux, and Philippe Leclère**

Presently, metallic nanowires (NWs) are the most promising materials to fabricate flexible transparent electrodes as an alternative to indium tin oxide. Here, the high performance of transparent conductive electrodes (TCEs) based on silver nanowires (AgNWs) percolation networks is reported. With optimized experimental conditions for the deposition, the AgNWs result in low sheet resistance of 10 Ω sq^{-1} combined with a high optical transmittance of 92.6% at $\lambda = 550$ nm. This leads to a valuable figure of merit as compared to other TCEs. In this study, the nanoscale electrical properties of the AgNWs are measured via conductive atomic force microscopy to characterize the percolation network. The electrical resistivity value calculated for a single AgNW is found to be about 12.35 μΩ cm, while a nanoscale conductivity map over an AgNW network bridging two electrodes has revealed high levels of current within the network over a distance of more than 1000 μm. The favorable determined conductivity results along with the high optical properties of the AgNWs network strongly suggest that thin-film electrodes based on AgNWs will be a potential approach for future flexible electronic devices.

1. Introduction

In recent years, transparent conductive electrodes (TCEs) have attracted considerable attention for their use as components of optoelectronic devices such as flexible touch screens,[1,2] flexible heaters,[3–6] touch sensors,[7] supercapacitors,[8] organic light-emitting diodes (OLEDs),[9–11] or thin-film solar cells.[12–15] Consequently, there is a major need to fabricate TCEs with low sheet resistance (R_s) and high optical transmittance to reach optimum performance for various electronic applications.[16] Due to its low sheet resistance (10–20 Ω sq^{-1}) and high transmittance (up to 90%), indium tin oxide (ITO) is the most widely used transparent electrode material in optoelectronic devices.[14,17] However, ITO suffers from its high cost, scarcity of indium, and mechanical brittleness.[12,18,19] This issue has motivated the search for low-cost TCEs, such as Al-doped ZnO,[20] graphene,[21,22] carbon nanotubes (CNTs),[9,23] and metal nanowires (NWs),[24,25] to replace ITO. In particular, silver nanowires (AgNWs) networks providing excellent optical transparency, high electrical conductivity, and outstanding mechanical properties are most promising to be alternatives for future applications in flexible optoelectronic devices.[16,24,26] However, the high contact resistance of silver nanowires and the effect of the insulating poly(vinyl pyrrolidone) (PVP) coating, commonly used as a surfactant during the AgNW synthesis, strongly affect the performance of AgNW-based transparent electrodes. Therefore, further processing steps necessary to remove this insulation and improve contacts between the nanowires are required.[19]

Many processing techniques have been reported to optimize the electrical resistance, like mechanical pressing,[27] plasmon

S. H. Pham, R. Lazzaroni, P. Leclère
Laboratory for Chemistry of Novel Materials
Center for Innovation and Research in Materials and Polymers (CIRMAP)
Research Institute in Materials Science and Engineering University of Mons (UMONS)
Mons B-7000, Belgium
E-mail: philippe.leclere@umons.ac.be

S. H. Pham, A. Ferri, A. Da Costa, M. M. S. Mohan, R. Desfeux
Univ. Artois
CNRS
Centrale Lille
Univ. Lille
UMR 8181 – UCCS – Unité de Catalyse et Chimie du Solide
Lens F-62300, France

S. H. Pham, P. Leclère
Laboratory for Physics of Nanomaterials and Energy
Research Institute in Materials Science and Engineering
University of Mons (UMONS)
Mons B-7000, Belgium

V. D. Tran, D. C. Nguyen
International Training Institute for Materials Science (ITIMS)
Hanoi University of Science and Technology
No. 1 Dai Co Viet, Hai Ba Trung, Hanoi 100 000, Vietnam

P. Viville
Materia Nova R&D Center
Mons B 7000, Belgium

The ORCID identification number(s) for the author(s) of this article can be found under https://doi.org/10.1002/admi.202200019.

DOI: 10.1002/admi.202200019

Table 1. Characteristics of the three types of AgNWs used in this study.

	Diameter [nm]	Length [µm]	Concentration [mg mL^{-1}]
AgNW50	50	100–200	1
AgNW60	60	10–20	4
AgNW115	115	30–50	1

welding,[28] laser sintering,[29] chemical treatment,[29–31] metal oxide coating, or reinforcing the junction by glue.[32,33] Some of these methods require power input and energy consumption, while others may raise problems that could damage chemically sensitive substrates. Recent studies demonstrated that thermal annealing could improve electrical resistance by welding nanowires.[34–36] However, the effects of the annealing process on the nanowire network have not been clearly described at the nanoscale.

In this work, we report on high-performance transparent electrodes based on silver nanowire networks fabricated via the spin-coating method. These layers show both high transparency and conductivity, associated with excellent reproducibility. Furthermore, for the first time, the current spreading through the overall AgNW network was investigated by means of a nanoscale probing tool, namely conductive atomic force microscopy (c-AFM).

2. Results and Discussion

2.1. Morphology of Silver Nanowire

In the present work, three different sets of TCE samples, hereafter called AgNW50, AgNW60, and AgNW115 according to the NW-diameter (**Table 1**), were fabricated and then finely characterized. These samples were prepared via different spin-coating cycles (from one to five cycles). For the NW-based transparent electrodes, the most critical parameter to adjust is the interconnection between nanowires. As shown in **Figure 1**a, the sheet resistance decreases gradually as the number of spin-coating cycles increases. Indeed, the density of nanowires networks increases as a function of the number of cycles, thereby significantly improving the conductivity of the TCEs. For the AgNW50, we see that three cycles are already sufficient to reach low values of R_s. In contrast, in the case of AgNW60 and AgNW115 samples, the sheet resistance values are too high when two cycles of spin-coating are applied, meaning that the nanowire surface coverage is not good enough to create an efficient percolation pathway. One reason is most probably the fact that AgNW60 and AgNW115 are much shorter. When the spin-coating step was repeated from three to five times, the R_s reduced from 232 and 87 Ω sq^{-1} (three layers) to 37 and 26 Ω sq^{-1} (five layers) for these two materials, respectively. The sheet resistance of AgNW50 is lower than for AgNW60 and AgNW115, decreasing from 73 Ω sq^{-1} (one layer) to 20.5 Ω sq^{-1} (three layers). From these results, applying three spin-coating cycles was selected as the optimal process to prepare AgNWs TCE for our further investigations. In addition, the heat treatment of the AgNWs film also has a significant effect on the electrical properties of the TCEs.[36] The annealing treatment was strategically used to improve the interconnection between the AgNWs in the networks, allowing for a significant reduction of the TCEs resistance at an optimal temperature. As shown in Figure 1b, the optimal annealing temperature of the AgNW50 and AgNW60 samples is 165 °C. After 1 h of annealing at 165 °C, the sheet resistance of these samples decreased from 20.5 (AgNW50) and 37.0 (AgNW60) down to 10.6 and 20.5 Ω sq^{-1}, respectively. Due to the influence of the nanowire diameter, the AgNW115 required a higher temperature for this annealing step. Its sheet resistance reduced from 83.0 to 28.0 Ω sq^{-1} after 1 h of treatment at 200 °C. Besides, all types of nanowires easily tend to form a spherical ball-like structure at higher temperatures, which is due to the Rayleigh instability phenomenon, which breaks at the junction, thereby the R_s values of all three samples were significantly increased when raising the annealing temperature from 200 to 300 °C. This effect of the Rayleigh instability was observed in Figure S1c,f,i (Supporting Information) at 300 °C, as highlighted by the red arrows. This phenomenon occurs when atomic diffusion is enhanced as the temperature increases, the nanowires then tend to reduce their surface energy, and eventually, the silver nanowire networks cannot maintain the percolation threshold leading to a loss of conductivity.[36] For a given wire, the heat flux received by the silver will depend on its mass, i.e., its volume which will be a function of its diameter squared multiplied by its length. AgNW50 and AgNW115 have an average volume of the same order of magnitude, while AgNW60 have a volume ten times smaller. This is why this last one presents the worst instability phenomenon. Figure 1c represents the evolution of the sheet resistance as a function of the annealing time from

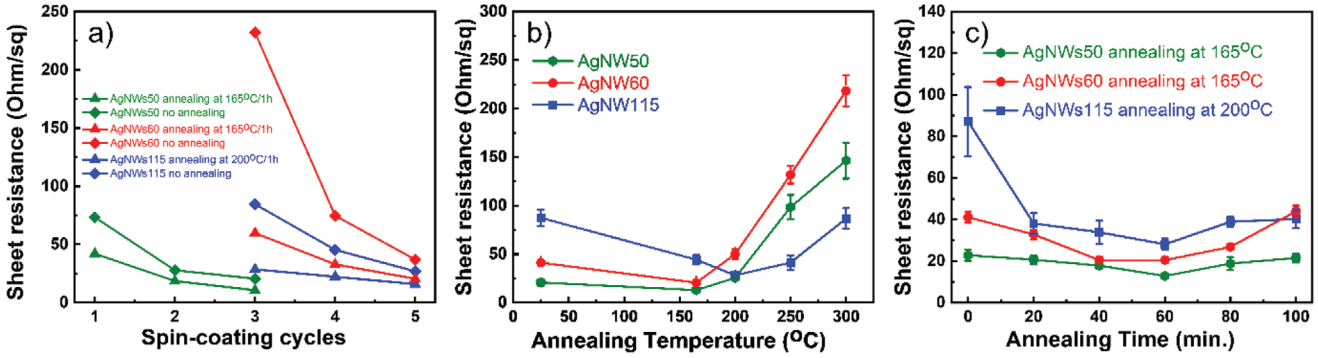

Figure 1. Electrical properties of the AgNW-based electrodes. a) Sheet resistance of three types of AgNW50, AgNW60, and AgNW115 samples with different spin-coating cycles onto the glass substrate. Evolution of sheet resistance as a function of annealing b) temperature and c) time.

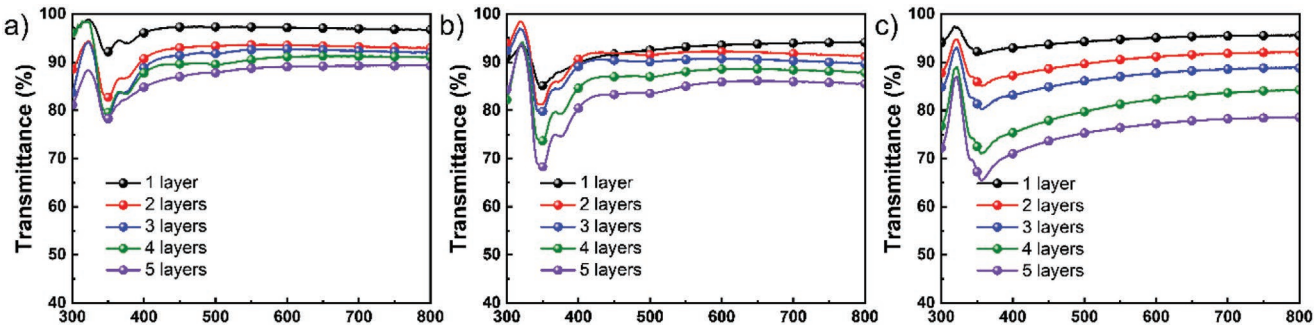

Figure 2. Optical properties of the AgNW-based electrodes. Transmittance of the a) AgNW50, b) AgNW60, and c) AgNW115 films for different deposited layers.

0 to 100 min, showing that the resistance decreases rapidly in the first stage. The resistance decreases slowly till 60 min of annealing then increases after more extended heat treatment above 60 min. This trend is observed because the AgNWs start to coalesce, breaking the electrical connections.[37] The effect of the thermal treatment on the morphology of the nanowires network was observed by SEM imaging and is shown in Figure S1 (Supporting Information). For comparison, the uniform and random orientation of the network is made of AgNW50, AgNW60, and AgNW115. Before the annealing process is shown in Figure S1a,d,g (Supporting Information), respectively. The global resistance of TCEs based on metallic nanowires is mainly due to the resistances at the NW junctions ($R_{NW} \ll R_j$, where R_{NW} and R_j are the electrical resistances of a single nanowire and at a nanojunction, respectively).[38] An apparent beneficial effect of thermal treatment on the interconnection of the AgNWs network is illustrated in Figure S1b,e,h (Supporting Information). First, the temperature annealing process improves the wire–wire junctions, reducing the sheet resistance significantly. Tapping mode (TM)-AFM images of intersecting AgNWs before and after thermal treatment are shown in Figure S2 (Supporting Information), evidencing heating-induced fused nanowires allowing for improved network connectivity. Furthermore, the PVP insulating layers are removed at high temperatures, also strongly reducing the resistance of TCEs.[39] Such annealing conditions were applied for the samples described below.

2.2. Optical Properties

The optical transmittance of the AgNW50, AgNW60, and AgNW115 films was studied for different thicknesses obtained by varying the number of spin-coating cycles, as depicted in **Figure 2**a–c. After the annealing process, all the films showed excellent transparency in the visible region, as revealed by the high transmittance values. As the spin-coating cycles increased, the nanowire density and the number of AgNWs cross-junctions increased, which induces a decrease in the optical transmittance. At the wavelength of 550 nm, the best-measured transmittance for AgNW50, AgNW60, and AgNW115 is 92.6%, 90.6%, and 87.2%, respectively. These values are higher than commercial ITO TCEs (86%).[40] In addition, we note a negligible change in transmittance before and after thermal treatment (see Figure S3, Supporting Information). These outstanding high transmission values evidence the suitability of such AgNWs-based thin film transparent electrodes for electronic devices. Ideally, in applications such as transparent conductive films, optical transmittance, and electrical conduction should be as large as possible. However, there is an antagonism between those two properties, which excludes the simultaneous achievement of an optimal transmittance and optimal electrical conduction in most cases.

To assess the performances of our TCE thin films and compare them with published results, we have considered the typical figure of merit (FoM), defined as the ratio of electronic (σ_{DC}) to optical (σ_{Op}) conductivity. In the bulk-like regime, where the conductivity is invariant with the film thickness, the following usual formula is used[31]

$$\frac{\sigma_{DC}}{\sigma_{Op}} = \frac{Z_0}{2R_s \times \left(T_{550}^{-\frac{1}{2}} - 1\right)} \quad (1)$$

T_{550} is the transmittance at the wavelength of 550 nm, R_s is the sheet resistance of the TCEs (unit Ω sq^{-1}), and Z_0 is the free space impedance (377 Ω). This FoM expression is generally used for TCEs exhibiting high optoelectronic properties. The calculated values for our NWs are shown in **Figure 3**.

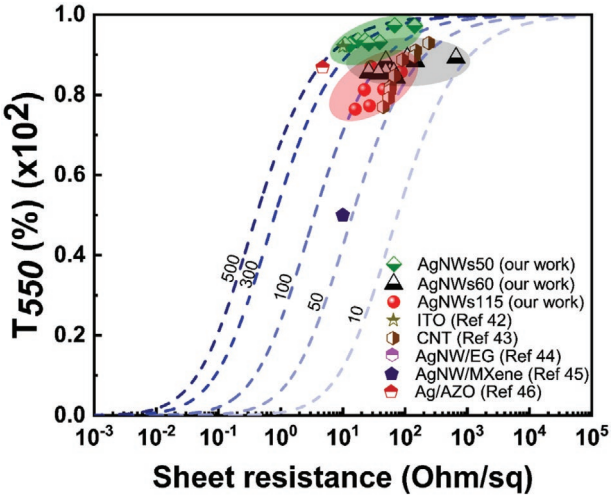

Figure 3. Figure of merit of the fabricated TCEs. Transmittance ($\lambda = 550$ nm) plotted as a function of sheet resistance for the AgNW networks studied, and compared to relevant systems reported in the literature.

The highest FoM value, obtained for AgNW50 (with three layers), i.e., with long nanowires, is ≈400, which is found to be higher than that of other electrodes, including ITO,[41] carbon nanotubes (ITO/SWCNT),[42] AgNW/EG (exfoliated graphene),[43] or AgNW/MXene,[15] but is slightly lower than that of AZO (Al-doped ZnO)/AgNWs.[44] The long nanowires could be interconnected with a lower coverage density, allowing for higher transmission with the same sheet resistance. These results point to the fact that the use of appropriate silver NWs, along with optimal recipes for deposition and post-treatment, allows for the fabrication of very high-quality TCEs that could be exploited in advanced optoelectronic applications.

2.3. Nanoscale Electrical Properties

For better understanding the excellent global electrical conductivity measured for the AgNWs networks depicted above, the charge transport was locally investigated by using c-AFM. Indeed, the nanoscale current percolation pathways govern the macroscopic conductivity of the network, making crucial both the visualization and the control of these AgNWs. All the current measurements presented in the following were obtained from AgNW50-based samples, previously described as the networks exhibiting the highest FoM values. **Figure 4**a illustrates the c-AFM measurement setup that was used to probe the electrical properties of the AgNWs network. The current pattern and the surface morphology of the nanowires network were simultaneously recorded to assess the conductivity behavior then demonstrate the detail of electrical performances at the nanoscale. The large-scale SEM image is shown in Figure 4b reveals that these nanowires randomly contact the ITO electrode, demonstrating compatibility and suitability for characterizing the electrical properties at such a local scale. To probe the conduction behavior of the AgNW networks, an external bias voltage ranging from 0 up to 900 mV was applied to the ITO electrode (Figure 4d–h). The measuring position of the AFM tip was 500 µm away from the ITO electrode to eliminate the effect of the nanowire lattice surface. We define lattice surfaces as nanowires whose ends are facing upward, not on the same plane as other nanowires. Due to a spin-coating, a random nanowire network is formed between the two ITO electrodes. The tendency is that the nanowire tips can point upward due to the weight of the nanowire network between the two ITO electrodes. Therefore, we cannot eliminate this factor, so to limit the influence in the measurement process, we choose a survey location about 500 µm away from the ITO electrode for survey purposes. The c-AFM technique is a two-terminal measurement. Therefore, the resistance at the contact points between the nanowire and the grounded probe is almost impossible to

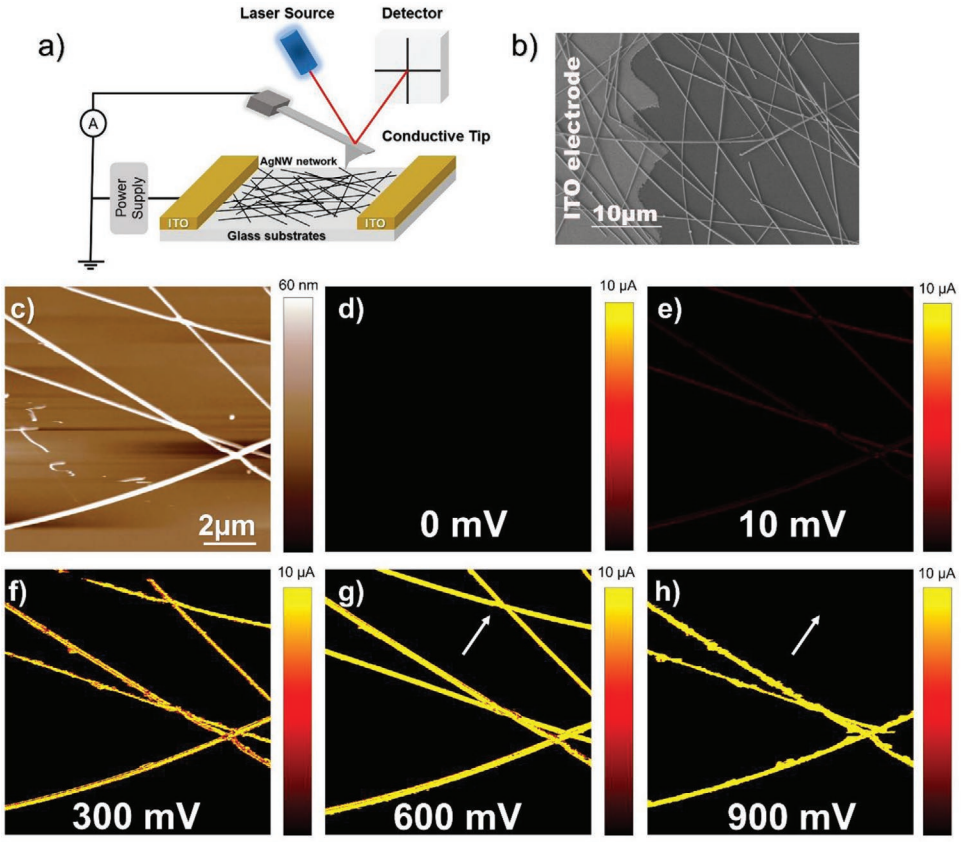

Figure 4. Nanoscale measurement of the electrical properties of the AgNW50-based electrodes. a) Schematic illustration of c-AFM setup and b) SEM image of the studied AgNWs/ITO sample. c) AFM topographic image, and d–h) corresponding c-AFM patterns for applied bias voltage of 0, 10, 300, 600, and 900 mV, respectively. White crosses seen in (g) and (h) refer to the rupture of AgNWs due to the electrical breakdown occurring at high voltage. 10 µA is the detection limit of our current module.

eliminate. However, as reported by Nirmal-raj et al., it is still comparable when applying the same force between the AFM probe and the electrode during all current measurements,[45] which is the case in this work. The nanowire diameter was found to be ≈80–100 nm from the c-AFM experiments performed in contact mode (Figure 4c), which is larger than the "true" nanowire diameter (≈50 nm) recorded by TM-AFM (see Figure S2, Supporting Information). The small deviation is due to the larger radius of the tip, owing to the presence of the conductive coating, known as the AFM tip convolution. Hence, the width of the nanowire in the conductive region is wider than the actual diameter of the nanowire due to the conduction expanding with outward deviation when the AFM probe contacts the nanowire.[46] The detected current is depicted in Figure 4d–h as a function of the applied bias voltage (see Figure S4, Supporting Information, for corresponding AFM topographic images).

The high contrasts attributed to local electrical conductivity evidence that the nanowires and electrodes are physically well contacted and are consistent with the excellent macroscopic performances of the AgNWs-based electrodes. As a remark, we observe that the nanowires tend to rupture owing to the electrical breakdown occurring at high voltage estimated at 900 mV, as revealed by the white arrows in Figure 4g,h. The disappearance of the current signal for such electrical bias is due to the disruption of the electrical contact where the new segment of AgNW is isolated and then no longer contributes to the current flow in the network. This phenomenon is highlighted in Figure S5 (Supporting Information). Consequently, all c-AFM measurements presented below were performed by applying a bias voltage of 600 mV.

2.4. Local Electrical Behavior of Single AgNWs

To estimate the resistivity of an individual AgNW, an AgNW50-based solution was diluted to a lower concentration and coated at high speed to obtain a lower surface coverage and favoring the presence of single nanowires connected to the lateral ITO electrode, as shown in **Figure 5**a. As mentioned above, we cannot suppress the resistance that affects the current measurements, such as contact resistances at the ITO electrode and AFM tip, thus from the detected signal, the total measured resistance (R_{tot}) can be described as a linear series of resistors and calculated according to the following equation

$$R_{tot} = R_{NW} + R_j + R_{other} \quad (2)$$

where R_{other} is the combined resistance of the network and the contact, R_{NW} is the electrical resistance of a single nanowire, while R_j is the resistance of a nanojunction. The resistivity of the AgNW (ρ) is calculated by using the equation

$$\rho = \frac{R_{NW} \times S}{l} \quad (3)$$

Here, l is the distance from the ITO electrode to the measurement position obtained from the AFM topographic signal (Figure 5a). To accurately assess to the resistivity, we chose four locations (labeled to A, B, C, and D on the conductivity image (Figure 5b) precisely separated by 500 nm along the nanowire axis. In addition, we also have to precisely determine the geometrical parameters of the nanowire. It is well-known that the growth of AgNWs leads to a regular pentagonal structure from (111) planes in the case of the polyol synthesis with PVP. In our case, we have experimentally determined the nanowire diameter from the AFM height profiles along the individual AgNW presented in Figure 5a for each of the four positions (A–D). The average experimental value is found to be 51.7 nm, as expected for such AgNW50 sample, allowing us to calculate the cross-sectional area of the pentagonal structure (S). Then, by considering the well-known Pouillet's law mentioned above, the resistivity of the AgNW50 was estimated for various distances along the nanowire. The resistivity value at the position measurement is determined by taking the average value of the cross section through the measuring point. The detailed calculation and the determined values related to the different locations along the Ag nanowire are summarized in Figure S6 (Supporting Information). These measurements have led to an average value for the resistivity of 12.35 μΩ cm. This value is larger than the bulk silver (0.16 μΩ cm),[47] which has been previously explained by the combined effect of different structural and phonon scatterings.[48] In the case of AgNWs, both phonon and structural scatterings contribute to the higher resistivity measured here.

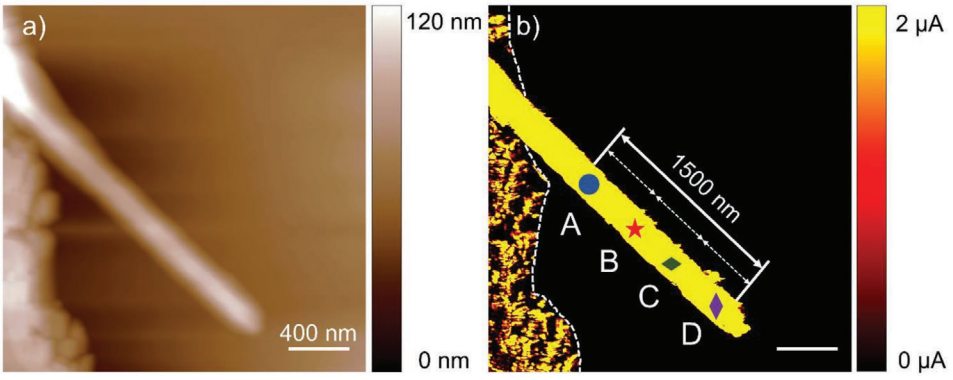

Figure 5. Local conductivity of individual AgNW contacted to ITO electrode. a) AFM morphology and b) c-AFM current signal simultaneously recorded over a single AgNW50.

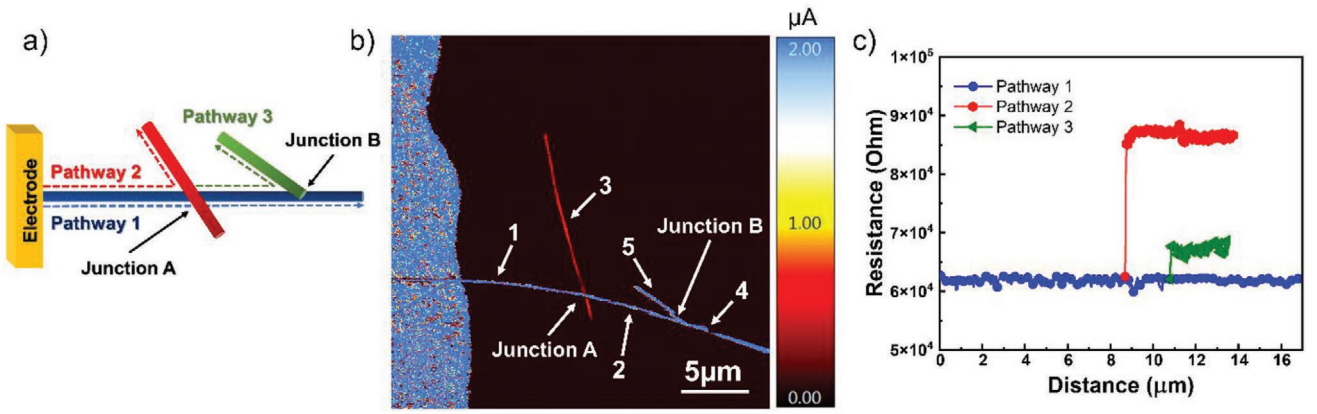

Figure 6. Resistance behavior of different nanojunctions in AgNWs film. a) Schematic of analyzed conductive pathways. b) The current pattern of a main AgNW contacted to electrode and displaying two kinds of nanojunctions. c) Electrical resistance evolution of the conductive pathways, strongly dependent on the X- or Y-junctions.

It is noteworthy that our estimated resistivity value is in perfect agreement with the theoretical calculations from Bloch–Grüneisen's theory previously reported for similar AgNWs of 50 nm in diameter[49] or with the experimental values published for AgNWs of 227 nm in diameter.[48] Consequently, the c-AFM technique is shown here to be suitable for probing electronic transport properties in our transparent conductive films, enabling the measurements presented hereafter. Besides, this is the first report on the nanoscale determination of electrical resistivity for a single AgNW.

2.5. Local Electrical Behavior of AgNWs Network

The electrical resistances of the nanojunctions are crucial for the global performances of AgNW-based TCEs, as they usually govern the transport properties of the overall network. To determine these resistance values, we have set up the measuring system illustrated in **Figure 6**a, where a main individual nanowire is electrically connected to the electrode but is also connected to two other nanowires, providing two different nanojunctions (X or Y configuration) here labeled A and B. In this specific configuration, the current flowing long three different pathways (numbered 1, 2, and 3) related to the two types of junctions, here A and B, as illustrated in Figure 6a. The current mapping recorded in this configuration is shown in Figure 6b, where two main current contrasts are revealed: a higher signal (blue color) is measured both for the main AgNW connected to ITO as well as for the segment connected at the B-junction, while a lower current signal (red color) originates from the A-junction. By determining the resistance at the positions (1-2) & (1-3) and (2-4) & (2-5) marked in Figure 6b, we eliminate the effect of the other resistance measurements, which allows for the calculation of the resistance at a single junction. The resistance values are found to be about 8.5×10^4 and 6.6×10^4 Ω for A- and B-junctions, respectively. As expected, the resistances at nanojunctions are much higher than for single nanowires. The obtained differences for the junction resistances are explained by the poorer contact area of the A-type junction compared to the B-junction, as already reported in the previous studies.[45] In this case, owing to the lower quality of electrical contact between the two nanowires offered by junction A, pathway 2 involves fewer electronic charges. At the B-junction, no significant change in the recorded c-AFM contrast is shown in Figure 6b, resulting in a much smaller increase of the resistance value (Figure 6c), in full agreement with the Y-type junction more suitable for the efficient conducting network. In this latter case, the contact area is higher, inducing low contact resistance. This result illustrates the different resistance behaviors for these two very specific nanojunctions. However, the determined values cannot be considered as the average value of all the junctions of the entire conductive network. In addition, it is worth noting that the determined junction resistance is also dependent on the single nanowire diameter and the bundles comprising the junction.

To evidence the quality of nanowires connections on the macroscopic scale as well as to describe the global lateral conductivity spreading through the fabricated network, the AgNWs were deposited between two ITO electrodes separated by 1000 μm, as illustrated schematically in **Figure 7**a and shown by the SEM image on Figure 7b. The first ITO electrode is directly connected to the bias voltage produced by the AFM instrument and referred to as "connected electrode," whereas the opposite ITO electrode is labeled "non-connected electrode." A set of 10×10 μm^2 areas have then been probed with c-AFM at increasing distances (≈0, 200, 400, 600, 800, and 1000 μm) from the connected ITO electrode. The current patterns are presented in Figure 7c–h, where the two electrode edges are represented by the white dotted lines on the first and last c-AFM images (Figure 7c,h). Regardless of the distance from the connected electrode, the AgNWs appear highly conductive in the current patterns, with values reaching several micro-amps (≈10 μA). These current patterns demonstrate the excellent charge transport behavior through the whole network up to the remote unconnected electrode, as seen on the right side of Figure 7h. We believe that this study is describing with more details the electrical mapping of AgNW network by c-AFM previously studied by De et al. in 2009.[50]

This result further underlines the high performance of the AgNW-based TCEs fabricated in this present work. **Figure 8**a

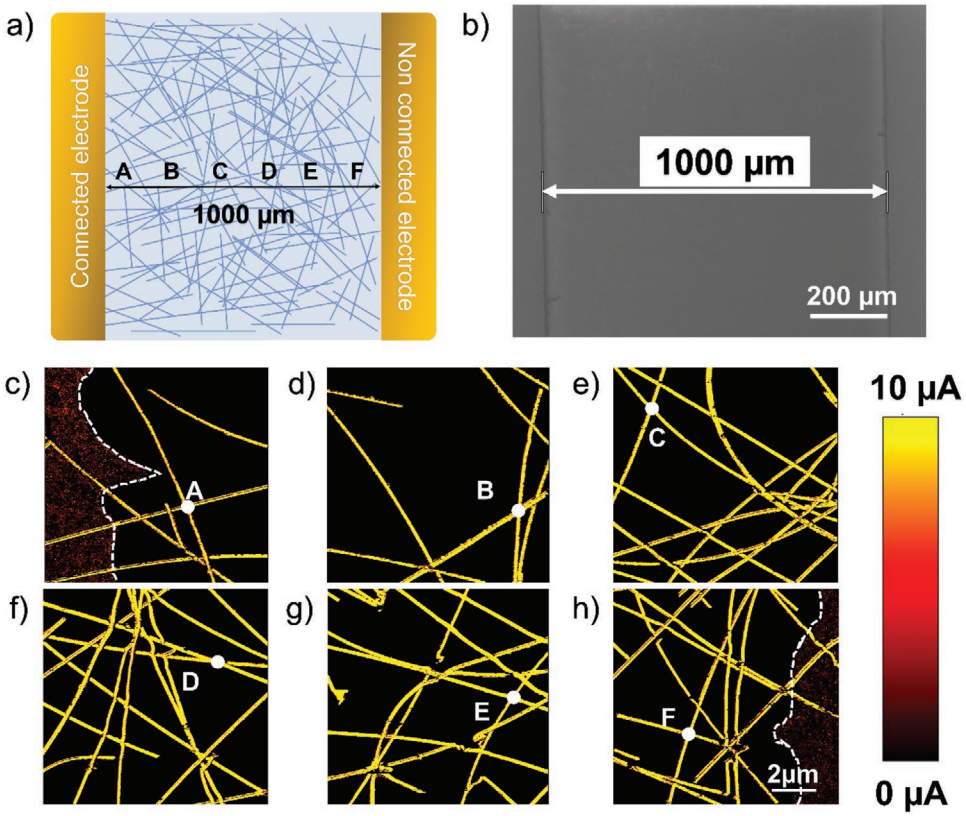

Figure 7. Nanoscale electrical conductivity spreading in the global AgNW50-based network. a) Schematic illustration of the "electrical bridge" based on AgNWs and b) SEM image of the large conductive region probed between the two lateral ITO electrodes. c–h) c-AFM current mapping of various areas of the AgNWs network, each on related to A, B, C, D, E, and F regions specified in (a) between connected (left-side) and unconnected (right-side) electrodes.

shows the typical nanoscale *I–V* curves recorded on different nanojunctions identified as A, B, C, D, E, and F on Figure 7c–h, respectively. The results reveal that the higher the connected electrode-probing tip separation, higher the electrical resistance, as depicted by the decreasing of the *I–V* characteristics slope when moving away from the connected electrode. The resistance values deduced from each recorded *I–V* curve are plotted in Figure 8c, where a non-linear trend is obtained. Indeed, a clear quadratic behavior is observed, which may be related to the increase in nanojunctions density measured throughout the entire conducting nanowire network from the c-AFM tip to the connected electrode, as well by the random nature of the probed junctions (X- or Y-configuration).

In this case, the number of junctions would increase quadratically along with the network, i.e., with the distance from the connected ITO. This result would reveal more a topology issue than a materials property issue. On the other hand, the lower current detected for both lateral electrodes (1 and 2) in Figure 8a

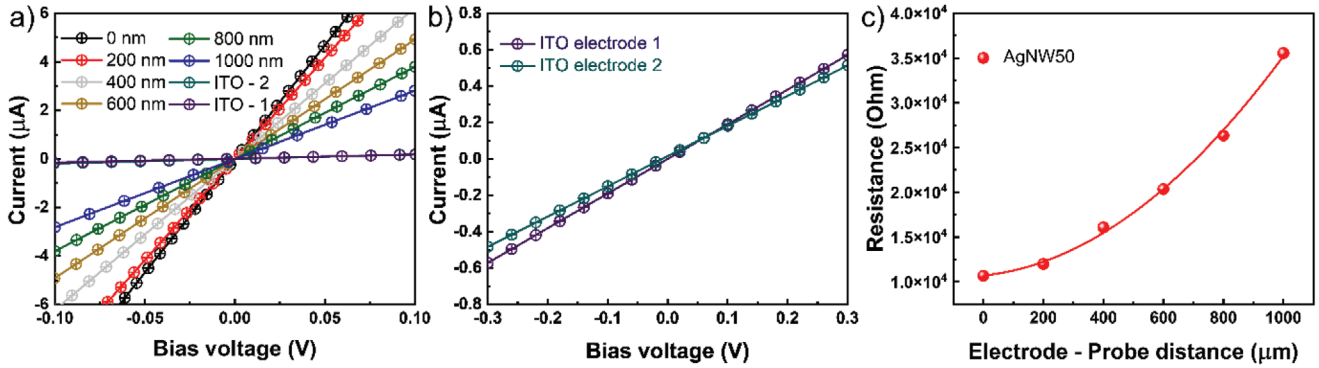

Figure 8. Local *I–V* characteristics analysis of the AgNW50-based network. a) Local *I–V* curves were recorded at the points labeled from A to F in Figure 7c–h. b) Zoom of the *I–V* curves directly measured over both the "connected" (Figure 7c) and "unconnected" (Figure 7h) ITO electrodes. c) Evolution of the resistance values determined from *I–V* curves as a function of the connected electrode–probe distance.

reveals the higher resistive nature of the semiconducting ITO material compared to the conducting metallic AgNWs, combined to the lower contact area for lateral electrode–AFM tip interface compared to the nanowire–AFM tip contact. Besides, the comparison of the *I*–*V* curves measured over the two opposite electrodes presented in Figure 8b exhibits no significant change in transport behavior. The later result reveals the high transport properties through the overall network and suggests these conducting thin films based on AgNWs could be potential candidates to efficiently replace the ITO-based TCE.

3. Conclusion

To conclude, in this study, TCEs based on AgNW networks were successfully fabricated by spin-coating. The effects of the temperature and the time during the annealing process on optoelectronic properties were investigated on the different types of AgNWs. The best result showed a sheet resistance of 10 Ω sq^{-1} with a transmittance of 92.6% at a wavelength of 550 nm, equivalent to the highest FoM value of 400. This very interesting value allows for the use of these TCEs in numerous electronic organic applications, such as OLED or thin-film solar cells devices. The electrical resistivity value calculated for a single strand AgNW50 using c-AFM is about 12.35 μΩ cm, consistent with the simulation results reported in the literature. Different resistance behaviors were detected for two specific types of nanojunctions, namely, X and Y, usually observed in such metallic nanowire networks. A nanoscale conductivity map over an AgNW network bridging two ITO electrodes has revealed high current levels within the network over a distance of more than 1000 μm. A quadratic behavior for the nanojunctions resistance values through the entire network was evidenced, explained by the junction number, which increases quadratically along with the network. This study emphasizes the simple fabrication and processing technologies to optimize the network connectivity of AgNW-based transparent electrodes and paves the way for novel electrode materials to replace metal oxides as transparent conductors for advanced electronic devices.

4. Experimental Section

Materials: The AgNWs solutions were purchased from Sigma Aldrich and ACS Materials. Three types of AgNWs were used with the average diameter and length of 50, 60, and 115 nm, and 100–200, 10–20, and 30–50 μm, respectively (see Table 1). The calculated ratios between length and diameter (*L*/*D*) are 2000–4000, 167–333, and 260–435, representing long, short, and medium nanowires, respectively. Other chemicals used from commercial products were refined to analytical purity.

Fabrication of AgNWs TCEs: The AgNW TCEs were fabricated by spin-coating. Before deposition, the substrates were treated with O_2 plasma cleaning in a vacuum for 10 min to form a hydrophilic surface. First, the glass substrate was thoroughly cleaned by ultrasonication, followed by three successive washings in acetone and isopropyl alcohol (IPA), and dried with pure N_2 at high pressure. The AgNW solution was diluted in IPA to a concentration of 1 mg mL^{-1}. Typically, a 150 μL AgNWs suspension was spun on a glass substrate (2 × 2 cm^2) at 700 rpm for 30 s with different spin-coating cycles (from one to five cycles), then the film was dried at 80 °C for 5 min to evaporate the solvent fully. Then each type of AgNW network was annealed in a vacuum at different optimal temperatures in the range from 165 to 200 °C for 1 h to improve the contact between the AgNWs and to remove residual PVP.

For the c-AFM investigation of the local electrical properties of the AgNW, glass/ITO substrates were used to connect the nanowires to a contact ITO electrode. The cleaning process for glass/ITO (Naranjo substrate, ref NS1463, ITO 95 nm-thick, ≈20 Ω sq^{-1}) was performed sequentially in demineralized water, detergent (RBS), acetone, IPA, for 10 min in a sonication bath and dried with pure N_2 at high pressure. Then oxygen plasma treatment was applied on the surface of the ITO electrode for 5 min. Finally, the deposition process of the AgNWs was similar to that just described above.

Characterization: The sheet resistance of TCEs was measured by four-point probe system measurements (Keithley Standard Series 2400). The reported values were taken as the average of at least 8–10 measurements from random positions on the sample surface. The optical transmittance measurements were performed with a Shimazu ultraviolet–visible (UV–vis) spectrophotometer in wavelengths ranging from 300 up to 800 nm. The surface morphologies and structures of the AgNW network were analyzed using a field emission scanning electron microscope (FESEM, Hitachi S4800).

An AFM measurement system using a Dimension Icon instrument (Bruker Nano Inc., Santa Barbara, CA) in TM-AFM was selected for characterizing the microstructural properties of both the single nanowires and the fabricated networks. An MFP-3D instrument (Asylum Research/Oxford Instruments, USA) was used to locally investigate the electrical conductivity by means of the c-AFM mode. For such experiments, the measurements were conducted in contact mode at room temperature in air with a conductive probe that is continuously moving over the sample surface at a constant scan rate of 0.3 Hz, ensuring stability in the current detection. Diamond-coated silicon tip and cantilever with a nominal 9 N m^{-1} spring constant (CDT-CONTR-10, Nanosensors) were used, and the sample–tip interaction nominal force was kept constant to 10 nN. In this case, the tip was grounded, and the bias voltage was applied to the bottom electrode (ITO layer).

Supporting Information

Supporting Information is available from the Wiley Online Library or from the author.

Acknowledgements

The authors are grateful to the Région Hauts-de-France, to the FRS-FNRS (Belgium), to the Fonds Européen de Développement Régional (FEDER), to the Ministère de l'Enseignement Supérieur, de la Recherche et de l'Innovation (France), to the Major Domain of Interest (DIM) "Eco-Energy Efficiency" of Artois University, and to the University of Mons for supporting and funding partially this work. Région Hauts-de-France and FEDER are also acknowledged for funding the MFP-3D microscope under Program "Chemistry and Materials for a Sustainable Growth."

Conflict of Interest

The authors declare no conflict of interest.

Data Availability Statement

The data that support the findings of this study are available from the corresponding author upon reasonable request.

Keywords

annealing treatment, conductive atomic force microscopy (c-AFM), silver nanowires, transparent electrodes

Received: January 4, 2022
Revised: March 1, 2022
Published online: March 31, 2022

[1] S. Cho, S. Kang, A. Pandya, R. Shanker, Z. Khan, Y. Lee, J. Park, S. L. Craig, H. Ko, *ACS Nano* **2017**, *11*, 4346.
[2] B. Deng, P. C. Hsu, G. Chen, B. N. Chandrashekar, L. Liao, Z. Ayitimuda, J. Wu, Y. Guo, L. Lin, Y. Zhou, M. Aisijiang, Q. Xie, Y. Cui, Z. Liu, H. Peng, *Nano Lett.* **2015**, *15*, 4206.
[3] D. Kim, L. Zhu, D. J. Jeong, K. Chun, Y. Y. Bang, S. R. Kim, J. H. Kim, S. K. Oh, *Carbon* **2013**, *63*, 530.
[4] J. Kang, H. Kim, K. S. Kim, S. K. Lee, S. Bae, J. H. Ahn, Y. J. Kim, J. B. Choi, B. H. Hong, *Nano Lett.* **2011**, *11*, 5154.
[5] K. H. Pyo, J. W. Kim, *Compos. Sci. Technol.* **2016**, *133*, 7.
[6] N. M. Nair, J. K. Pakkathillam, K. Kumar, K. Arunachalam, D. Ray, P. Swaminathan, *ACS Appl. Electron. Mater.* **2020**, *2*, 1000.
[7] N. M. Nair, K. Daniel, S. C. Vadali, D. Ray, P. Swaminathan, *Flexible Printed Electron.* **2019**, *4*, 045001.
[8] Q. Jiang, N. Kurra, M. Alhabeb, Y. Gogotsi, H. N. Alshareef, *Adv. Energy Mater.* **2018**, *8*.
[9] Z. Z. Gu, Y. Tian, H. Z. Geng, D. S. Rhen, A. S. Ethiraj, X. Zhang, L. C. Jing, T. Wang, Z. H. Xu, X. T. Yuan, *Appl. Nanosci.* **2019**, *9*, 1971.
[10] L. Lian, X. Xi, D. Dong, G. He, *Org. Electron.* **2018**, *60*, 9.
[11] M. Choi, Y. J. Park, B. K. Sharma, S. R. Bae, S. Y. Kim, J. H. Ahn, *Sci. Adv.* **2018**, *4*, eaas8721.
[12] A. Kim, H. Lee, H.-C. Kwon, H. S. Jung, N.-G. Park, S. Jeong, J. Moon, *Nanoscale* **2016**, *8*, 6308.
[13] A. Kim, Y. Won, K. Woo, C. H. Kim, J. Moon, *ACS Nano* **2013**, *7*, 1081.
[14] K. P. Sibin, G. Srinivas, H. D. Shashikala, A. Day, N. Sridhana, A. K. Sharma, H. C. Barshilia, *Sol. Energy Mater. Sol. Cells* **2017**, *172*, 277.
[15] H. Tang, H. Feng, H. Wang, X. Wan, J. Liang, Y. Chen, *ACS Appl. Mater. Interfaces* **2019**, *11*, 25330.
[16] Y. Chen, R. S. Carmichael, T. B. Carmichael, *ACS Publ.* **2019**, *11*, 31210.
[17] S. H. Liu, H. W. Yu, Q. Y. Zhang, F. S. Qin, X. Zhang, L. T. Zhang, W. F. Xie, *J. Mater. Chem. C* **2019**, *7*, 5426.
[18] S. Shi, V. Sadhu, R. Moubah, G. Schmerber, Q. Bao, S. Ravi, P. Silva, *J. Mater. Chem. C* **2013**, *1*, 1708.
[19] D. S. Hecht, L. Hu, G. Irvin, *Adv. Mater.* **2011**, *23*, 1482.
[20] J. I. Nomoto, T. Hirano, T. Miyata, T. Minami, *Thin Solid Films* **2011**, 1400.
[21] Y. S. Yun, D. H. Kim, B. Kim, H. H. Park, H. J. Jin, *Synth. Met.* **2012**, *162*, 1364.
[22] J. Ha, S. Park, D. Kim, J. Ryu, C. Lee, B. H. Hong, Y. Hong, *Org. Electron.* **2013**, *14*, 2324.
[23] J. Lee, M. Lim, J. Yoon, M. S. Kim, B. Choi, D. M. Kim, D. H. Kim, I. Park, S. J. Choi, *ACS Appl. Mater. Interfaces* **2017**, *9*, 26279.
[24] M. Göbelt, R. Keding, S. W. Schmitt, B. Hoffmann, S. Jackle, M. Latzel, V. V. Radmilovic, V. R. Radmilovic, E. Spiecker, S. Christiansen, *Nano Energy* **2015**, *16*, 196.
[25] S. Ye, A. R. Rathmell, Z. Chen, I. E. Stewart, B. J. Wiley, *Adv. Mater.* **2014**, *26*, 6670.
[26] T. Sannicolo, M. Lagrange, A. Cabos, C. Celle, J. P. Simonato, D. Bellet, *Small* **2016**, *12*, 6052.
[27] T. Tokuno, M. Nogi, M. Karakawa, J. Jiu, T. T. Nge, Y. Aso, K. Suganuma, *Nano Res.* **2011**, *4*, 1215.
[28] J. Lee, J. Y. Woo, J. T. Kim, B. Y. Lee, C. S. Han, *ACS Appl. Mater. Interfaces* **2014**, *6*, 10974.
[29] J. A. Spechler, K. A. Nagamatsu, J. C. Sturm, C. B. Arnold, *ACS Appl. Mater. Interfaces* **2015**, *7*, 10556.
[30] Y. Yang, S. Chen, W. Li, P. Li, J. Ma, B. Li, X. Zhao, Z. Ju, H. Chang, L. Xiao, H. Xu, Y. Liu, *ACS Nano* **2020**, *14*, 8754.
[31] S. Lee, J. Jang, T. Park, Y. M. Park, J. S. Park, Y. K. Kim, H. K. Lee, E. C. Jeon, D. K. Lee, B. Ahn, C. H. Chung, *ACS Appl. Mater. Interfaces* **2020**, *12*, 6169.
[32] Q. H. Tran, D. T. Chu, V. H. Hoang, S. H. Pham, P. Leclère, T. T. H. Nguyen, D. H. Tran, Q. T. Do, A. T. Pham, D. C. Nguyen, *Mater. Lett.* **2021**, *287*, 129243.
[33] A. T. Pham, X. Q. Nguyen, D. H. Tran, V. N. Phan, T. T. Duong, D. C. Nguyen, *Nanotechnology* **2016**, *27*, 335202.
[34] T. Bin Song, Y. Chen, C. H. Chung, Y. Yang, B. Bob, H. S. Duan, G. Li, K. N. Tu, Y. Huang, *ACS Nano* **2014**, *8*, 2804.
[35] D. Y. Choi, H. W. Kang, H. J. Sung, S. S. Kim, *Nanoscale* **2013**, *5*, 977.
[36] M. Lagrange, D. P. Langley, G. Giusti, C. Jiménez, Y. Bréchet, D. Bellet, *Nanoscale* **2015**, *7*, 17410.
[37] J. Y. Lee, S. T. Connor, Y. Cui, P. Peumans, *Nano Lett.* **2008**, *8*, 689.
[38] M. Jagota, N. Tansu, *Sci. Rep.* **2015**, *5*, 10219.
[39] D. P. Langley, M. Lagrange, G. Giusti, C. Jiménez, Y. Bréchet, N. D. Nguyen, D. Bellet, *Nanoscale* **2014**, *6*, 13535.
[40] K. P. Sibin, N. Selvakumar, A. Kumar, A. Dey, N. Sridhara, H. D. Shashikala, A. K. Sharma, H. C. Barshilia, *Sol. Energy* **2017**, *141*, 118.
[41] Z. Chen, W. Li, R. Li, Y. Zhang, G. Xu, H. Cheng, *Langmuir* **2013**, *29*, 13836.
[42] M. R. Golobostanfard, H. Abdizadeh, S. Mohammadi, M. A. Baghchesara, *Sol. Energy Mater. Sol. Cells* **2015**, *132*, 418.
[43] A. G. Ricciardulli, S. Yang, G. J. A. H. Wetzelaer, X. Feng, P. W. M. Blom, *Adv. Funct. Mater.* **2018**, *28*, 1706010.
[44] D. S. Ghosh, T. L. Chen, N. Formica, J. Hwang, I. Bruder, V. Pruneri, *Sol. Energy Mater. Sol. Cells* **2012**, *107*, 338.
[45] P. N. Nirmalraj, P. E. Lyons, S. De, J. N. Coleman, J. J. Boland, *Nano Lett.* **2009**, *9*, 3890.
[46] A. Kim, Y. Won, K. Woo, S. Jeong, J. Moon, *Adv. Funct. Mater.* **2014**, *24*, 2462.
[47] A. L. Dearden, P. J. Smith, D. Y. Shin, N. Reis, B. Derby, P. O'Brien, *Macromol. Rapid Commun.* **2005**, *26*, 315.
[48] Z. Cheng, L. Liu, S. Xu, M. Lu, X. Wang, *Sci. Rep.* **2015**, *5*, 10718.
[49] A. Bid, A. Bora, A. K. Raychaudhuri, *Phys. Rev. B: Condens. Matter Mater. Phys.* **2006**, *74*, 035426.
[50] S. De, T. M. Higgins, P. E. Lyons, E. M. Doherty, P. N. Nirmalraj, W. J. Blau, J. J. Boland, J. N. Coleman, *ACS Nano* **2009**, *3*, 1767.